



King Saud University

Arabian Journal of Chemistry

www.ksu.edu.sa
www.sciencedirect.com



ORIGINAL ARTICLE

Study of rheological behavior of a hybrid nano-lubricant (MWCNT-Al₂O₃ (20:80)/SAE40) using two-way laboratory method and response surface methodology



Mohammad Hemmat Esfe ^{a,*}, Soheyl Alidoust ^b, Davood Toghraie ^{c,*}

^a Department of Mechanical Engineering, Imam Hossein University, Tehran, Iran

^b School of Chemistry, Damghan University, Damghan, 36716-41167, Iran

^c Department of mechanical engineering, Khomeinishahr branch, Islamic Azad University, Khomeinishahr, Iran

Received 19 May 2022; accepted 14 December 2022

Available online 21 December 2022

KEYWORDS

Hybrid NLS;
Rheological conduct;
Viscosity;
SAE40 oil;
RSM;
experimental data

Abstract In this paper, the rheological performance of MWCNT-Al₂O₃ (20:80)/SAE40 hybrid nano-lubricant (HNL) investigated and analyzed with different methods. The ranges of temperature, shear rate and volume fraction of nanoparticles (NP) are T = 25–50 °C, $\dot{\gamma}$ = 666.5 s⁻¹ to 13330 s⁻¹ and φ = 0.0625–1 %. This study was conducted to investigate and determine the most optimal laboratory conditions in lubrication and provide a relationship to predict experimental data and investigate the effect of dispersion of NP on the base fluid (BF) and the average wall shear stress. The results show that in different laboratory conditions, the desired HNL flow behavior is pseudo-plastic, non-Newtonian. It is found that viscosity (μ_{nf}) decreases, increases and decreases with increasing temperature (T), φ and $\dot{\gamma}$, respectively. The highest increase 35.69 % in μ_{nf} is recorded in the studied conditions. A quadratic-three-variable model with a coefficient of determination R-Squared = 0.9993 is used in the response surface methodology (RSM) to predict the experimental data. μ_{nf} φ . The diagram of dynamic viscosity changes for this model under the influence of temperature, shear rate and volume fraction parameters was presented. Temperature parameter has the most effect on viscosity. The theoretical method in this study reduces many laboratory costs and increases the speed of obtaining results.

© 2022 The Author(s). Published by Elsevier B.V. on behalf of King Saud University. This is an open access article under the CC BY license (<http://creativecommons.org/licenses/by/4.0/>).

* Corresponding authors.

E-mail address: Toghraee@iaukhsh.ac.ir (D. Toghraie).

Peer review under responsibility of King Saud University.



Production and hosting by Elsevier

1. Introduction

From the point of view of most researchers in the world, nanotechnology has been able to create many developments in the engineering sciences and various other branches in the last two decades, and for this reason, it is one of the interesting topics for researchers' research (Sun et al., 2021; Du et al., 2022; Wang et al., 2019; Cui et al., 2022; Tassew et al., 2022; Dwijendra et al., 2022; Mansouri et al., 2017; Suhad et al., 2021; Azin and Pourghobadi, 2021). Perhaps one of the most important applications of nanotechnology is in the field of fluid mechanics and heat transfer, which causes these two fields to have significant changes in indicators such as efficiency. Since ancient times, fluids were widely used in various fields such as heat transfer, lubrication, etc. (Putra, 2020; Wenhao et al., 2022; Yang et al., 2017; Li et al., 2022; Jia et al., 2022; Wang et al., 2022). Choi made the initial discovery of nanofluids (NFs) in 1995 at the National Argon Laboratory (ANL) (Choi and Eastman, 1995). Several investigators as innovators

in this subject have worked on the thermal properties of NFs as a new fluid by advanced attributes (Jafarimoghaddam and Aberoumand, 2016; Aberoumand et al., 2015; Aberoumand et al., 2016). The thermal conduct of NFs belongs to some main parameters like thermal conductivity (k_{nf}), viscosity (μ_{nf}), and heat capacity (Kole and Dey, 2010). Among the properties, the two properties of μ_{nf} and k_{nf} have attracted the most attention (Afrand et al., 2016; Akbari et al., 2017; Mahyari et al., 2019; Ruhani et al., 2019a,b, 2022). Most investigators have presented that the k_{nf} and μ_{nf} of NFs are higher than the BFs, because the addition of NPs increases the μ_{nf} and k_{nf} (Shahsavani et al., 2018; Yang et al., 2020; Nafchi et al., 2019) (See Fig. 1). By examining the rheological behavior of NFs, it is concluded that NPs not only increase the μ_{nf} but also alter the NFs from Newtonian to non-Newtonian (Dalkilic et al., 2016). Heat capacity plays a vital role in determining the capacity and performance of a fluid. The max the k_{nf} , the more heat can be transferred by liquids from systems. On the other hand, increasing the μ_{nf} in systems is important because the flow characteristics like Rey-

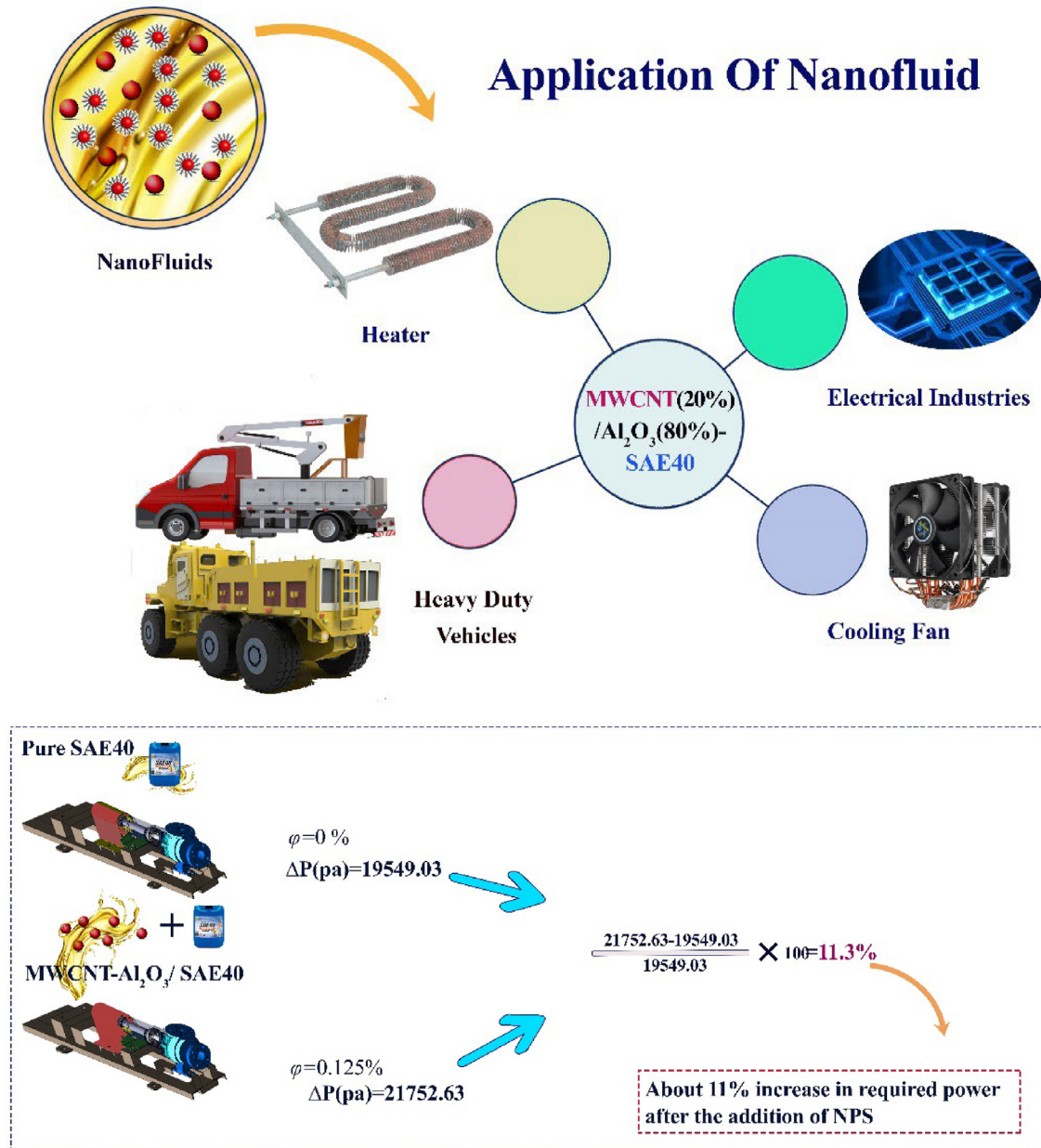


Fig. 1 Applications of NFs.

nolds number, heat transfer coefficient (HT), and pressure drop depend on the μ_{nf} (Siddiqui et al., 2019; Sidik et al., 2014). Also, the pipe geometry the through which the liquid flows is one of the significant parameters that can modify the rate of HT. Various pipe shapes can also increase HT, including secondary flow due to curvature in curved pipes and centrifugal force increasing the HT coefficient in spiral pipes (Razi, n.d.; Arani et al., 2016; Goharkhah et al., 2016). The use of helical tubes is one of the most common procedures for improving the HT of heat exchangers in many industries and devices such as heating systems, automotive industries, and power plants (Rakhsha et al., 2015). In helical tubes, the radial velocity is created by centrifugal force, and the flow of fluid outside the pipe is faster. This difference in velocity creates a secondary flow. Using spiral pipes instead of straight pipes, curved streamlines replace direct streamlines and increase HT, and as a result, the size of fluid flow pipes becomes smaller and the HT coefficient also increases (Mirgolbabaei et al., 2011; Jayakumar et al., 2010; Aly, 2014).

In addition to assessing the type and classification of fluids, researchers are interested in studying the trend of μ_{nf} changes and its response to independent variables such as T, φ and $\dot{\gamma}$. Table 1 reports the percentage increase in the μ_{nf} s with the addition of NPs in some studies.

Sujith et al. (Sujith et al., 2021; Sujith et al., 2019) investigated the rheological behavior of NLs in their recent studies. For example, they investigated the rheological behavior and density of MoS₂/sesame oil NLs. The results show that at different temperatures from 313 to 393 K, $\dot{\gamma}$ between 10 and 70 s⁻¹ and φ from 0.2 % to 1.2 %, the μ_{nf} and density of NLs increases with increasing φ and decreases with increasing temperature. In another study, investigating the viscosity of pure coconut oil/Al₂O₃ NLs with different φ of 0.2 % to 1.2 % was desired. By measuring the μ_{nf} , the effect of φ and temperature on the thermophysical properties of coconut oil/Al₂O₃ NLs was determined. Based on the results, the μ_{nf} of NLs decreases with increasing temperature, while it increases with increasing the number of NPs in the BF. Also, NLs show a relative viscosity > 1, which indicates the decisive effect of NPs desired NF. Hemmat's research group (HRG) has specialized in many of its studies (Esfe and Arani, 2018; Esfe and Sarlak, 2017; Esfe et al., 2022; Esfe et al., 2022) by using the RSM to forecast the thermophysical and rheological properties of different NFs. These studies forecast the μ_{nf} or k_{nf} of NFs, a new relation-

ship was presented that helps researchers to achieve results with high speed and accuracy without the need to spend exorbitant laboratory costs. In this examination, the changes in the conduct of rheological and comparison of μ_{nf} of MWCNT -Al₂O₃ (20:80)/ SAE40 HNL at various T, φ and $\dot{\gamma}$ were studied. HNLs will be contrasted in distinct parts by various targets in this investigation. In the initial section of the article, the kind of HNLs (Newtonian and non-Newtonian) is investigated with the offered procedures. In the next part, the role of the HNL state in the enhancement of the life of components and promotion is considered. Finally, to avoid reducing laboratory costs and time, as well as verifying the accuracy of modeling predictive data relative to experimental data by the RSM, a three-variable mathematical relationship (T, φ and $\dot{\gamma}$) was selected to forecast the μ_{nf} of the selected HNL. Eventually, the computation of the thermal performance for various conditions displays that the utilization of HNLs and coils of helical instead of the BF and straight pipes progresses the efficiency of HT.

2. Experimental process

2.1. Samples provision

For the purpose of experimental tests, first, using the desired NPs (purchased from Sigma Aldrich), HNLs with different φ are prepared. Fig. 2 shows the NPs. Eq. (1) was used to calculate the amount of NP samples at $\varphi = 0.0625$ %, 0.125 %, 0.25 %, 0.5 %, 0.75 % and 1 %.

$$w_{Al2O3orMWCNT} = \varphi \left[\left(\frac{w}{\rho} \right)_{Al2O3} + \left(\frac{w}{\rho} \right)_{SAE40} + \left(\frac{w}{\rho} \right)_{MWCNTorAl2O3} \right] \quad (1)$$

Table 2 lists some specifications of NPs.

To recognize the attributes of the morphology of NPs and SEM images and XRD were utilized to confirm the nanoscale. MWCNT and Al₂O₃ NPs of specified sizes were used in a specified combination ratio. Pictures of 2D and 3D XRD, and SEM of NPs are shown in Fig. 3.

Table 1 A review of the investigation on the... μ_{nf}

Ref.	NPs	BFs	The highest percentage change in μ_{nf}	lowest percentage change in μ_{nf}
(Moghaddam and Motahari, 2017)	MWCNT-CuO	SAE40	Maximum percentage change in μ_{nf} (at T = 50 °C and $\varphi = 1$ %) = + 75 %	Minimum percentage change in μ_{nf} (at T = 25 °C and $\varphi = 0.0625$ %) = + 0.19 %
(Esfe and Alidoust, 2020)	MWCNT-Al ₂ O ₃	5 W50	Maximum percentage change in μ_{nf} (at T = 55 °C, $\varphi = 1$ %) + 6 %	Minimum percentage change in μ_{nf} (at T = 15 °C, $\varphi = 0.05$ %) = -11 %
(Dardan et al., 2016)	MWCNT- Al ₂ O ₃	SAE40	Maximum percentage change in μ_{nf} (at T = 35 °C, $\varphi = 1$ %)= + 1.45 %	Minimum percentage change in μ_{nf} (at T = 50 °C, $\varphi = 0.0625$ %)= + 1.12 %
(Tian et al., 2020)	MWCNT- Al ₂ O ₃	10 W40	Maximum percentage change in μ_{nf} (at T = 65 °C, $\varphi = 1$ %) = 30.53 %	Minimum percentage change in μ_{nf} (at T = 25 °C, $\varphi = 0.05$ %) = 13.87 %
(Asadi et al., 2016)	MWCNT- MgO	SAE50	Maximum percentage change in μ_{nf} (at T = 40 °C, $\varphi = 2$ %)= + 65 %	Minimum percentage change in μ_{nf} (at T = 25 °C, $\varphi = 25$ %)= + 1404 %
(Liu et al., 2021)	MWCNT-TiO ₂	SAE20W40	Maximum percentage change in μ_{nf} (at T = 70 °C, $\varphi = 0.8$ %)= + 24.42 %	Minimum percentage change in μ_{nf} (at T = 20 °C, $\varphi = 0.1$ %)= + 5.75 %
(Chu et al., 2021)	MWCNT-TiO ₂	5 W40	Maximum percentage change in μ_{nf} (at T = 60 °C, $\varphi = 1$ %)= + 25 %	Minimum percentage change in μ_{nf} (at T = 20 °C, $\varphi = 0.05$ %) = -1%
(Afrand et al., 2016)	MWCNT-SiO ₂	SAE40	Maximum percentage change in μ_{nf} (at T = 50 °C, $\varphi = 1$ %)= + 25.8 %	Minimum percentage change in μ_{nf} (at T = 30 °C, $\varphi = 0.0625$ %)= + 9.92 %
(Binu et al., 2014)	MWCNT- TiO ₂	SAE40	Maximum percentage change in μ_{nf} (at T = 50 °C, $\varphi = 1$ %)= + 40 %	Minimum percentage change in μ_{nf} (at T = 25 °C, $\varphi = 0.05$ %) = 0 %

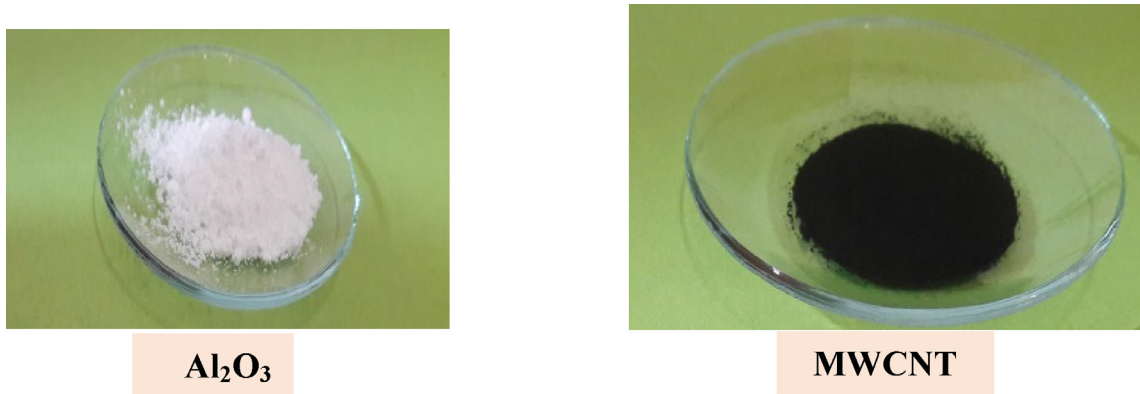


Fig. 2 The used NPs.

Table 2 Specifications of NPs.

NPs	Purity	Color	True density	APS	SSA	Morphology
MWCNTs	> 95 wt%	Black	~ 2.1 g/cm ³	ID: 3–5 nm OD: 5–15 nm ~ 50 um (Length)	> 233 m ² /g	Cylindrical
Al ₂ O ₃	≥ 99 %	White	3.97 g/cm ³	20 nm	138 m ² /g	nearly spherical

After weighing the NPs, to disperse the NPs to create the stable HNLs according to the two-stage technique, the magnetic stirrer was utilized for stability, prevent agglomeration, and sedimentation. Ultrasonic vibration was utilized to achieve excellent dispersion and stop the creation of NP clusters for 3 h. To stabilize the homogenized suspensions, they were located in an ultrasonic machine for 6 h. After around 3 weeks, solutions had no sedimentation, and HNLs were without sedimentation.

2.2. Measurement of μ_{nf}

After making the HNL, the viscometer CAP2000+ was utilized to gage the μ_{nf} . The operating conditions of the viscometer are given in **Table 3**. The μ_{nf} was gaged in various φ and at $T = 25^\circ\text{C}$ to 50°C in addition to $\dot{\gamma} = 666.5 \text{ s}^{-1}$ and 13330 s^{-1} . Before measuring the μ_{nf} , to confide the efficiency of the vis-

cometer and adjustment of the machine, the glycerin μ has experimented with at $T = 85.26^\circ\text{C}$, and it was seen that the acquired mistake was 93.2 %.

3. Outcomes and conversation

3.1. Conduct of rheological behavior

3.1.1. Influence of $\dot{\gamma}$

Fig. 4 shows the conduct of the rheological of NLs using the fitting of μ_{nf} - $\dot{\gamma}$ -shear stress curves. This curve simultaneously examines the effect of critical factors such as rate of shear and stress of shear on the μ_{nf} . In all φ , the μ_{nf} can be considered dependent on the two mentioned parameters. It seems that with increasing $\dot{\gamma}$, the μ_{nf} reduces slightly because of considerations of shear heating. With injecting φ , the μ_{nf} was enhanced, which shows the effect of φ . In this case, the dependence of the

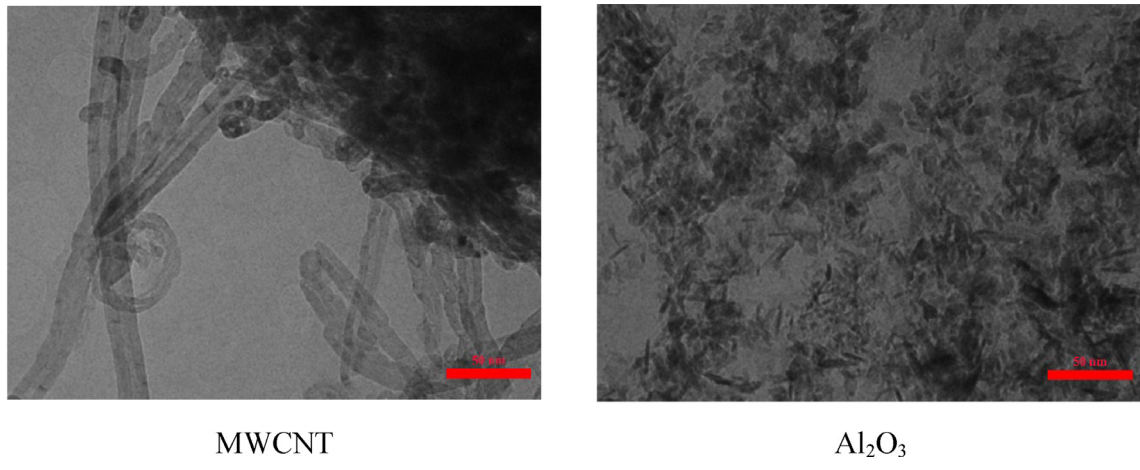
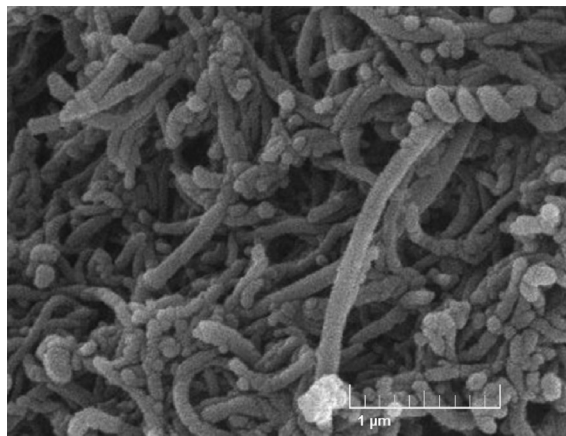


Fig. 3 Images of 2D and 3D XRD, and SEM of NPs.



MWCNT

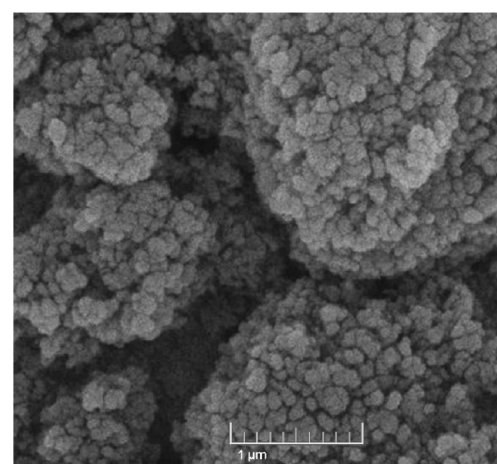
Al₂O₃

Fig. 3 (continued)

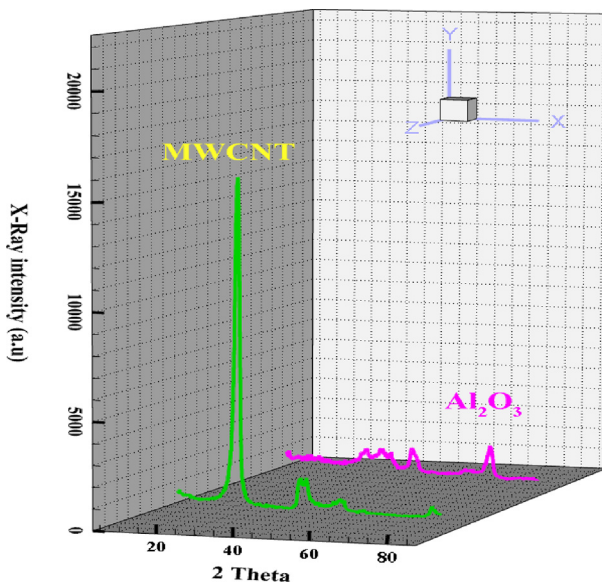


Fig. 3 (continued)

Table 3 Operating conditions of inputs viscometer CAP 2000 +.

Voltage (V)	In the range of 130 to 230
Frequency (Hz)	In the range of 50 to 60
Consumption of power (V)	< 345
Range of Torque	(dyne.cm) Low: 797–7970 (dyne.cm) High: 18000–18100
Speed (rpm)	In the range of 5 to 1000
T (C)	In the range of 5 to 75

μ_{nf} on the $\dot{\gamma}$ is slightly higher. Also, in the conduct of these diagrams, it can be observed that there is pseudo-plastic non-Newtonian conduct (He, 2020). Also, Hemmat Esfe research group in the past years (Esfe et al. 2018, Esfe et al. 2018) specifically and comprehensively investigated the rheological behav-

ior of different nanofluids. This phenomenon can be assigned to the mechanisms of the BF with the hybrid NPs and the creation of particular and intricate interactions among them. As φ increases, the influence of the variations is improved. Thus, non-Newtonian behavior emerges.

3.1.2. Index of power-law

If the conduct of rheological of NLs using the power-law model was considered, Eq. (2) (Esfe et al., 2022) could be used,

$$\tau = m\dot{\gamma}^n \quad (2)$$

The power-law model using n values determines the fluid behavior. In Fig. 5, the rheological behavior of the BF was compared with that of HNLs. Most of the change in HNL behavior occurs at $T = 45^\circ\text{C}$ and 50°C . At these T , the prepared HNL is more prone to strong non-Newtonian conduct. According to Fig. 5 and Table 4, the most non-Newtonian tendency of HNL behavior occurs under certain conditions ($\varphi = 1\%$ and $T = 45^\circ\text{C}$) with an index of power-law of 0.9259.

3.2. μ analogy

3.2.1. μ increasing

In Fig. 6, the μ -increasing and μ curves were merged based on the T variable and all φ . According to Table 5, which reports the statistical results of μ enhancement percentage, from $\varphi = 0.0625\%$ to $\varphi = 1\%$, approximately 33 % increase in μ_{nf} is observed. The lowest μ enhancement was 1.72 % at 500 RPM and $\varphi = 0.0625\%$ based on the outcomes.

$$\mu \text{ Enhancement (\%)} = \frac{\mu_{nf} - \mu_{bf}}{\mu_{bf}} \times 100 \quad (3)$$

3.2.2. The influence of T on μ_{nf}

Based on the curves in Fig. 7, which show the μ_{nf} at the lowest φ and the engine speeds of 300 and 500 RPM, it is possible to compare the NL conditions to the base oil to justify the using or not using nanomaterials. The curves in Fig. 7 show that the dispersion of MWCNT-Al₂O₃ (20:80) NPs increases the viscosity of BF. As a result, this HNL cannot be used to lubricate car engines at conditions similar to this study.

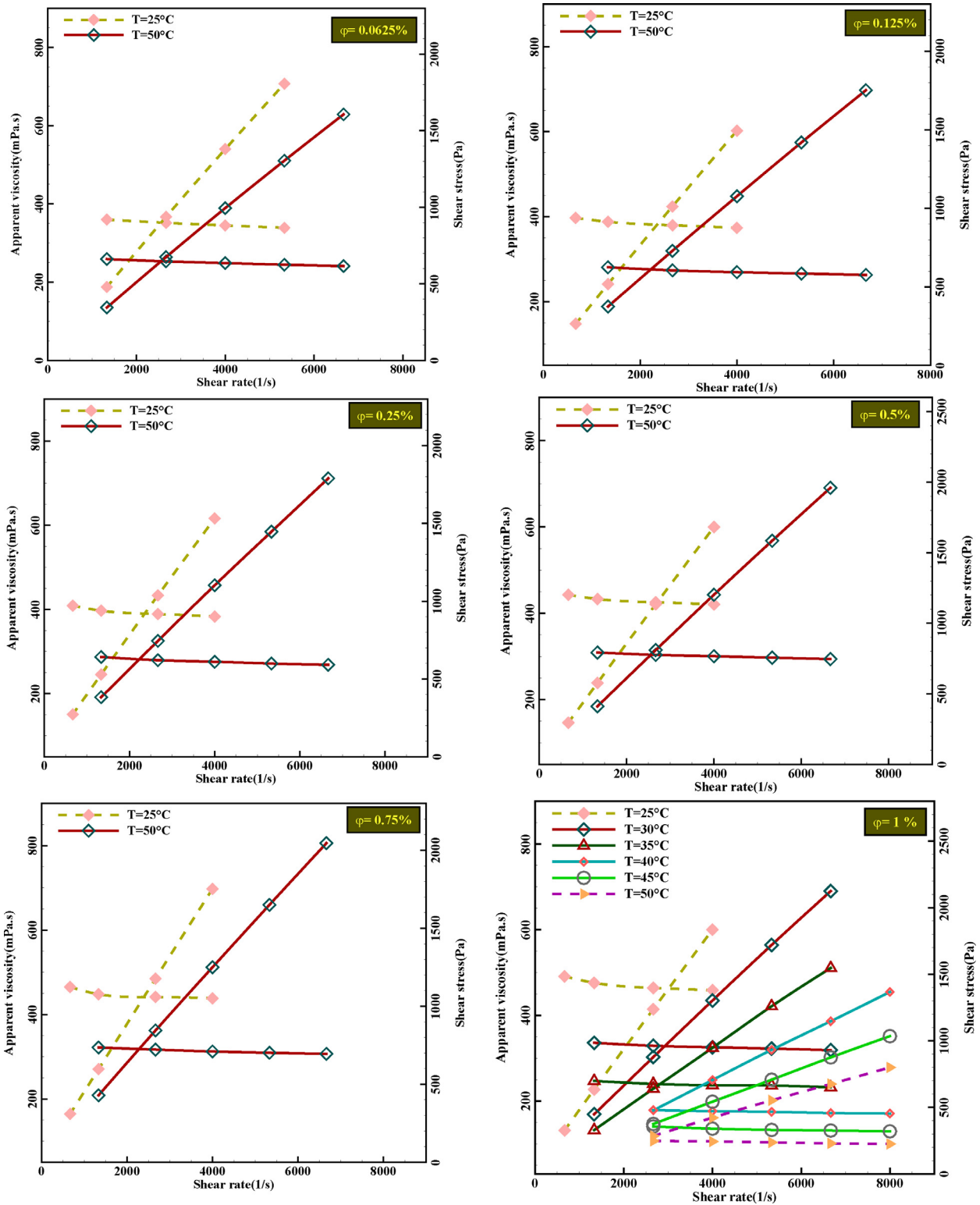


Fig 4 The μ_{nf} and stress stress versus.. $\dot{\gamma}$

The effects of T on μ_{nf} are reported numerically in Table 6. This can be assigned to different issues. One of them is the morphology of Al₂O₃ NPs and the use of a high percentage (80 %) of these NPs to prepare this HNL. Or the occurrence of a μ phenomenon in all test conditions may be due to factors

such as how the preparation is performed, stabilization of the HNL, or error of the tester. Because, in previous studies similar to this study, the opposite results were obtained (Esfe and Alidoust, 2020).

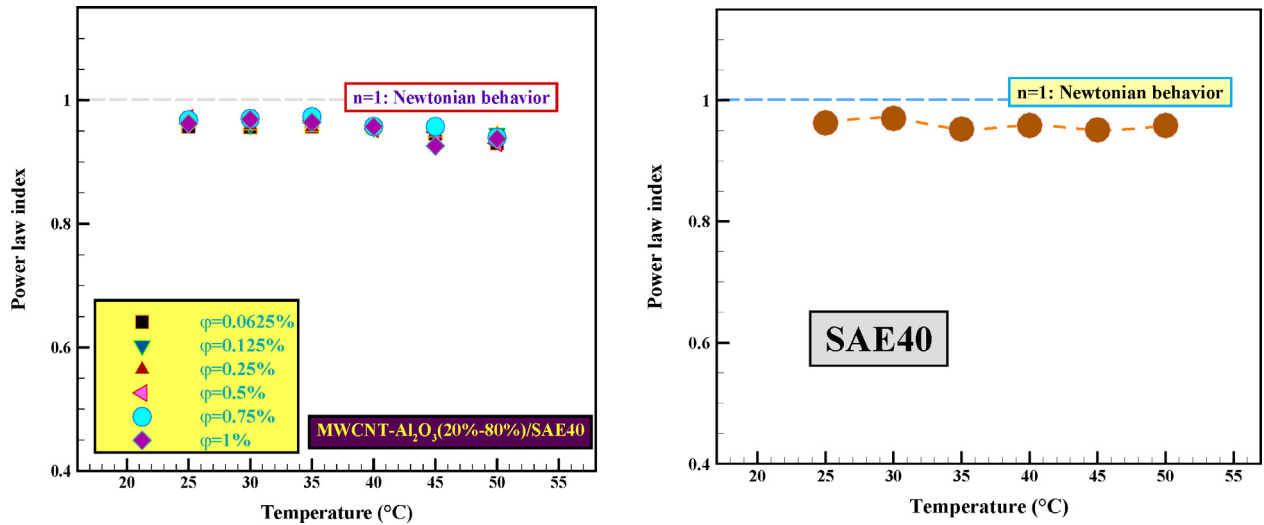


Fig. 5 Influence of T and φ on an index of power-law.

Table4 Index of Power-law amounts at various φ and T.

HNL T (°C)	$\varphi(\%)$	25	30	35	40	45	50
MWCNT-Al ₂ O ₃ (20:80)/SAE40	0.0625	0.9573	0.9562	0.9569	0.9554	0.9455	0.93
	0.125	0.9667	0.9594	0.9642	0.9556	0.9568	0.9463
	0.25	0.9643	0.9591	0.9565	0.9527	0.9481	0.9443
	0.5	0.9715	0.970	0.967	0.9528	0.9486	0.9301
	0.75	0.9676	0.9699	0.9729	0.9573	0.9571	0.9396
	1	0.962	0.9686	0.9641	0.9571	0.9259	0.9374
	0	0.9626	0.9701	0.9524	0.9585	0.9511	0.9584
SAE40	0						

4. Impractical outcomes

4.1. RSM method

RSM is one of the important procedures in examining the target response to achieve the relationship between the independent variable and the dependent variable. Using *Design of Experiment 11* software, T, $\dot{\gamma}$, φ input data and μ_{nf} output data were determined, and then, by processing the data, the desired model for predicting experimental data was extracted. A group of Chinese researchers investigated the properties of nanofluids theoretically and experimentally in their recent studies (Tu et al., 2022; Wang et al., 2022; Tu et al., 2022; Tang et al., 2022; Tu et al., 2022). They obtained good results using other new theoretical methods.

4.1.1. New correlation

In Eq. (4), the nonlinear predictive model based on three independent variables reports the output function. According to Eq. (4), the non-Newtonian conduct of the NL is quite obvious due to the dependence of the objective function on $\dot{\gamma}$. Also, the permissible range of use of Eq. (4) is Quartic model approved in the test conditions.

$$\begin{aligned}
 \mu_{nf} = & +2091.63454 - 135.27199T + 1087.50455\varphi \\
 & - 0.915170\dot{\gamma} - 48.28163T\varphi + 0.048131T\dot{\gamma} \\
 & + 0.135903\varphi\dot{\gamma} + 3.69980T^2 - 894.75544\varphi^2 \\
 & + 0.000805\dot{\gamma}^2 - 0.006557T\varphi\dot{\gamma} + 0.894265T^2\varphi \\
 & - 0.001111T^2\dot{\gamma} + 13.26694T\varphi^2 + 7.84976E \\
 & - 07T\dot{\gamma}^2 - 0.031861\varphi^2\dot{\gamma} + 0.000101\varphi\dot{\gamma}^2 \\
 & - 0.047939T^3 + 723.80181\varphi^3 - 1.41463E - 06\dot{\gamma}^3 \\
 & - 0.065438T^2\varphi^2 + 0.000032T^2\varphi\dot{\gamma} - 1.54938E \\
 & - 07T^2\dot{\gamma}^2 + 0.002812T\varphi^2\dot{\gamma} + 1.64761E - 07T\varphi\dot{\gamma}^2 \\
 & + 0.000023\varphi^2\dot{\gamma}^2 - 0.006039T^3\varphi + 9.44736E \\
 & - 06T^3\dot{\gamma} - 4.36444T\varphi^3 + 1.10655E - 08T\dot{\gamma}^3 \\
 & - 0.071143\varphi^3\dot{\gamma} - 8.49218E - 08\varphi\dot{\gamma}^3 + 0.000240T^4 \\
 & - 223.02133\varphi^4 + 5.62182E - 10\dot{\gamma}^4
 \end{aligned} \quad (4)$$

The normal probability diagram for the Quartic model is drawn in Fig. 8. Fig. 8 shows that the residuals follow the normal distribution of the data and the deviation between the data is very small and does not require an activation function.

Tables 7 and 8 show detailed statistical information on important parameters based on p-value and R-Squared values related to the selected model.

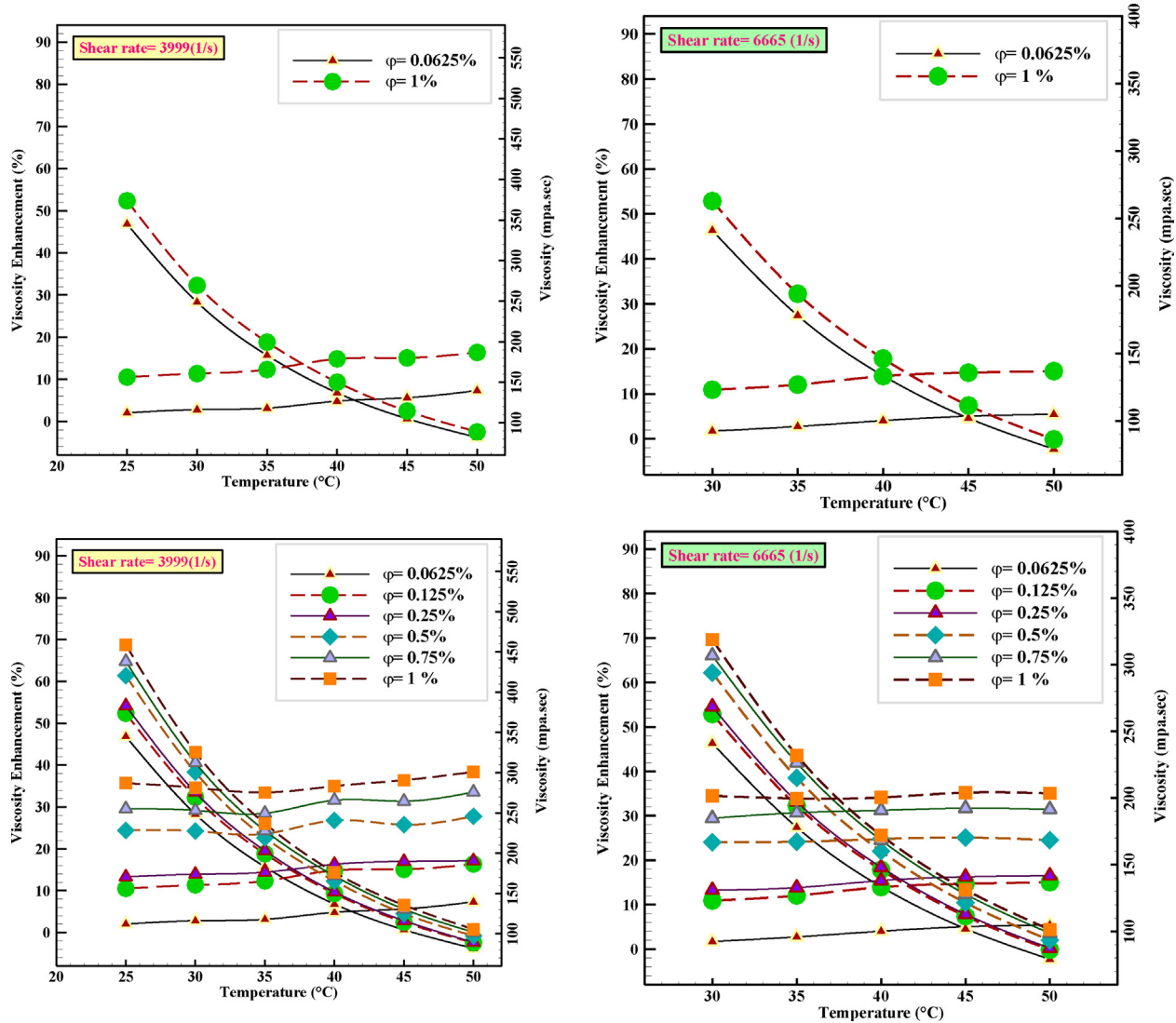


Fig. 6 μ enhancement applying φ at various T and $\dot{\gamma} = 3999$ and 6665 s^{-1} .

Table 5 Statistical information of MWCNT-Al₂O₃(20:80)/SAE40 HNL.

HNL	$\dot{\gamma}(\text{s}^{-1})$	T(°C)	$\frac{\Delta(\mu_{n-b})f}{\mu_{bf}} \times 100(\%)$
$\varphi(\%)$			
MWCNT-Al ₂ O ₃ (20:80)/SAE40	3999 (300 rpm)	T = 25	0.0625
		T = 30	2.04
		T = 35	2.81
		T = 40	3.15
	6665 (500 rpm)	T = 40	4.82
		T = 30	1.72
		T = 35	2.76
		T = 40	4.05
		T = 45	5.04
		T = 40	4.05
		T = 50	5.46
			0.125
			0.75
			1
			29.57
			29.18
			28.50
			31.62
			34.99
			29.45
			33.92
			31.25
			34.13
			31.71
			35.22
			31.25
			34.13
			31.46
			35.06

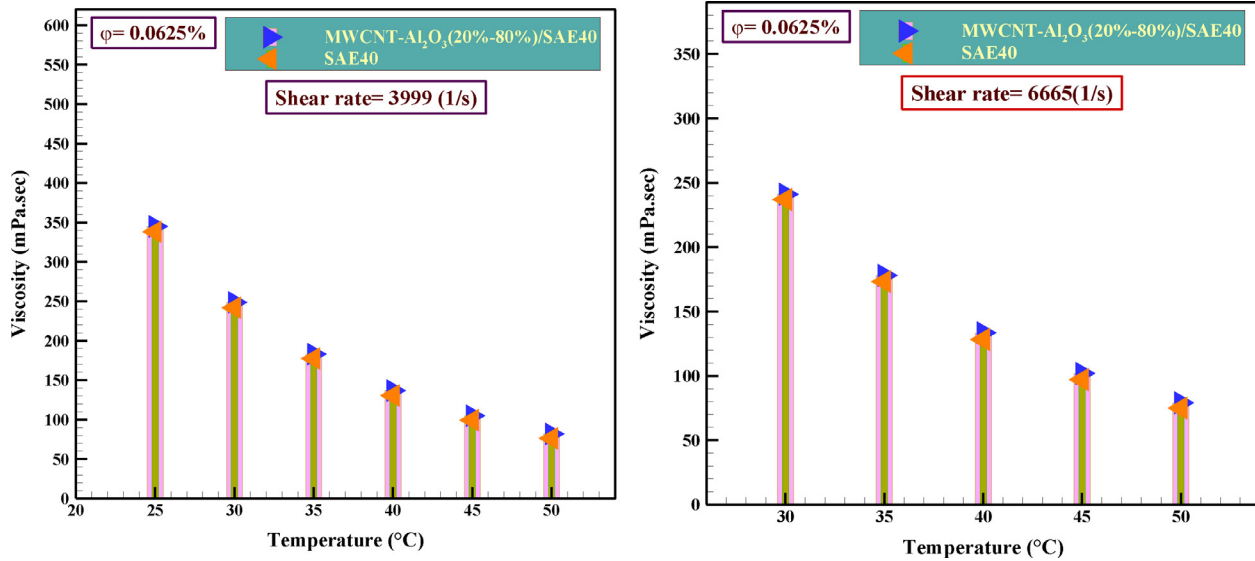


Fig. 7 The analogy of the influence of T on the μ_{nj} at $\varphi = 0.0625 \%$.

Table 6 Examination of the influence of T on the μ_{nj} relative to the BF at... $\varphi = 0.0625\%$

$\Delta(\mu_{n-b})_f$	T (°C)	$\dot{\gamma}(\text{s}^{-1})$
HNL		
6.90	25	
6.80	30	
5.60	35	3999
6.30	40	
4.80	35	
5.20	40	
4.90	45	6665
4.10	50	

Fig. 9 shows the evaluation of the predicted response values against the actual values. As you can see in **Fig. 9**, there is a slight deviation between the predicted data and the real data, and this indicates the high accuracy of this model.

4.1.2. Viscosity changes in the selected model

The viscosity changes of MWCNT-Al₂O₃ (20:80)/SAE40 nanofluid for the Quartic model were presented using laboratory data. With the help of the designed model, we analyzed the viscosity for different parameters. The trend of viscosity changes is drawn in figures 10 and 11. **Fig. 10** shows the trend of viscosity changes between temperature and volume fraction variables. As shown in the figure, viscosity increased with increasing temperature. But in **Fig. 11**, it shows the trend of changes in viscosity between temperature and cutting rate, and the viscosity has decreased slightly with increasing cutting rate.

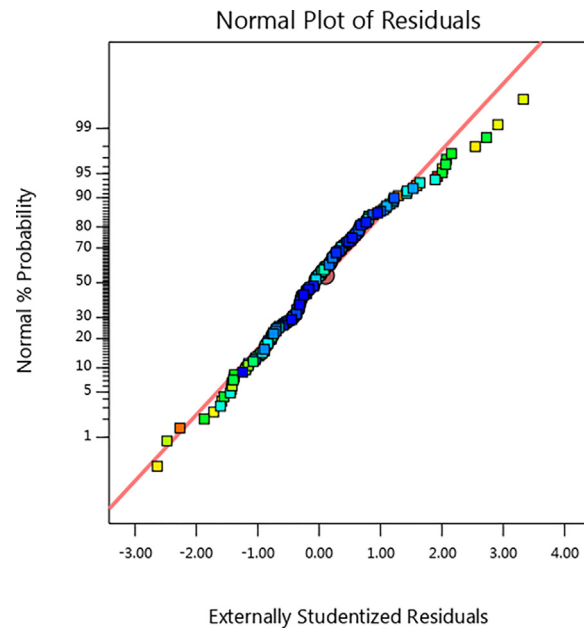


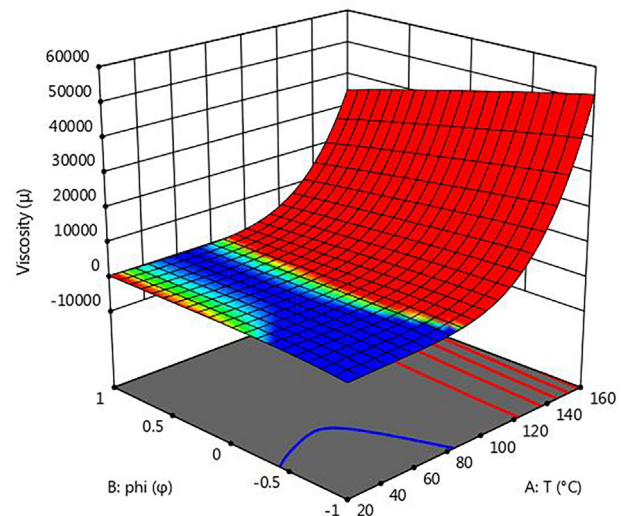
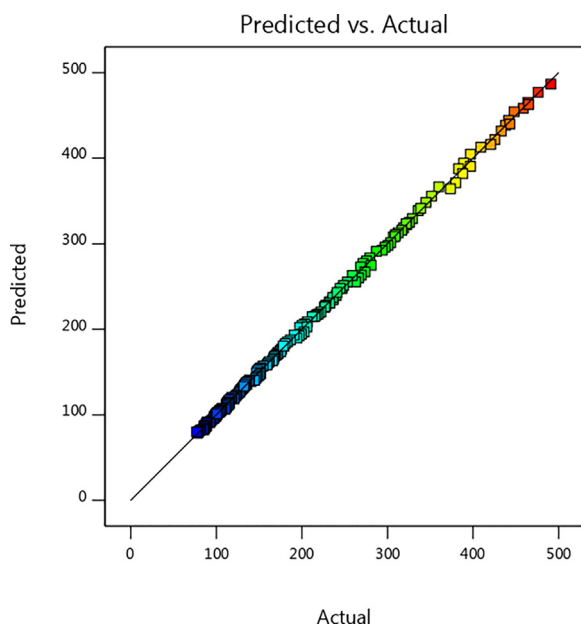
Fig. 8 Normal distribution curve in terms of residual values.

Table 7 Optimized modeling accuracy.

Std. Dev.	3.21	R ²	0.9993
Mean	207.16	Adjusted R ²	0.9991
C.V. %	1.55	Predicted R ²	0.9989
		Adeq Precision	282.8758

Table 8 ANOVA for RSM.

Source	Sum of Squares	df	Mean Square	F-value	p-value	
Model	2.013E + 06	34	59193.69	5728.71	< 0.0001	significant
A-T	23.37	1	23.37	2.26	0.1349	
B-phi	22.70	1	22.70	2.20	0.1405	
C-SR	8.46	1	8.46	0.8190	0.3670	
AB	33.79	1	33.79	3.27	0.0727	
AC	9.13	1	9.13	0.8831	0.3490	
BC	1.17	1	1.17	0.1132	0.7371	
A^2	25.63	1	25.63	2.48	0.1175	
B^2	2.63	1	2.63	0.2542	0.6149	
C^2	0.1042	1	0.1042	0.0101	0.9201	
ABC	0.0127	1	0.0127	0.0012	0.9721	
A^2B	39.97	1	39.97	3.87	0.0512	
A^2C	9.72	1	9.72	0.9410	0.3337	
AB^2	2.14	1	2.14	0.2070	0.6498	
AC^2	0.3739	1	0.3739	0.0362	0.8494	
B^2C	12.63	1	12.63	1.22	0.2707	
BC^2	0.0162	1	0.0162	0.0016	0.9684	
A^3	28.32	1	28.32	2.74	0.1001	
B^3	40.66	1	40.66	3.93	0.0493	
C^3	3.76	1	3.76	0.3635	0.5475	
A^2B^2	12.85	1	12.85	1.24	0.2668	
A^2BC	0.3421	1	0.3421	0.0331	0.8559	
A^2C^2	0.6492	1	0.6492	0.0628	0.8024	
AB^2C	5.43	1	5.43	0.5255	0.4697	
ABC^2	0.0026	1	0.0026	0.0002	0.9875	
B^2C^2	0.1940	1	0.1940	0.0188	0.8912	
A^3B	66.62	1	66.62	6.45	0.0122	
A^3C	10.57	1	10.57	1.02	0.3136	
AB^3	66.39	1	66.39	6.43	0.0124	
AC^3	1.06	1	1.06	0.1028	0.7489	
B^3C	6.70	1	6.70	0.6487	0.4219	
BC^3	0.5782	1	0.5782	0.0560	0.8134	
A^4	35.60	1	35.60	3.44	0.0656	
B^4	153.75	1	153.75	14.88	0.0002	
C^4	3.66	1	3.66	0.3541	0.5528	
Residual	1436.26	139	10.33			
Cor Total	2.014E + 06	173				

**Fig. 9** Comparison of predicted and actual values.**Fig. 10** Changes in nanofluid viscosity in terms of T and phi.

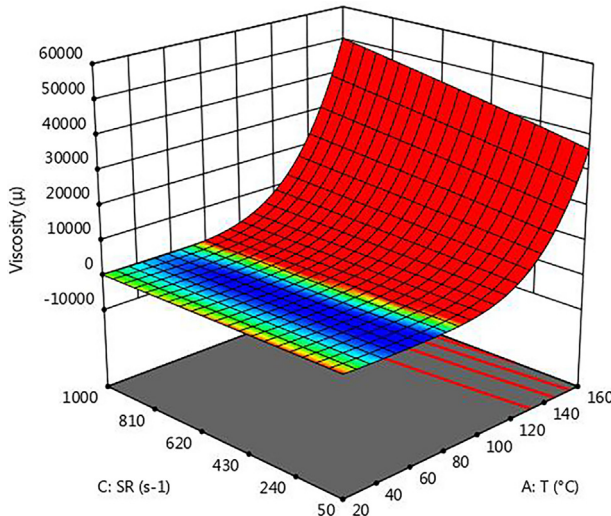


Fig. 11 Variations of nanofluid viscosity in terms of T and SR.

5. Conclusion

In summary, the rheological behavior of HNL was investigated with various procedures. A summary of important results is stated in the following cases:

- In different laboratory conditions, the HNL behavior is of the non-Newtonian type.
- μ_{nf} is inversely, directly, and inversely related to the independent variables of T, φ and $\dot{\gamma}$, respectively.
- With increasing NPs in the BF, the μ_{nf} increases significantly (35.69 %), while at lower T, the μ_{nf} decrease intensity increases.
- The μ_{nf} data were predicted with acceptable accuracy using the RSM and a four-point-three-variable model.
- The graph of changes in viscosity for Quartic model under the influence of parameters of temperature, shear rate and volume fraction was investigated, which shows that temperature parameter has the most effect on viscosity.

Declaration of Competing Interest

The authors declare that they have no known competing financial interests or personal relationships that could have appeared to influence the work reported in this paper.

References

- S. Aberoumand, K. Javaherdeh, A. Jafarimoghaddam, and H. Aberoumand, "Synthesis and rheological behavior of novel ecofriendly Ag–oil nanofluid and introduce general correlations for thermal conductivity and viscosity of any oil-based nanofluids," *Heat Trans Asian Res.* <https://doi.org/10.1002/htj>, vol. 21193, 2015.
- Aberoumand, S., Jafarimoghaddam, A., Moravej, M., Aberoumand, H., Javaherdeh, K., 2016. Experimental study on the rheological behavior of silver-heat transfer oil nanofluid and suggesting two empirical based correlations for thermal conductivity and viscosity of oil based nanofluids. *Appl. Therm. Eng.* 101, 362–372.
- Afrand, M., Najafabadi, K.N., Akbari, M., 2016. Effects of temperature and solid volume fraction on viscosity of SiO₂-MWCNTs/ SAE40 hybrid nanofluid as a coolant and lubricant in heat engines. *Appl. Therm. Eng.* 102, 45–54.
- Afrand, M., Toghraie, D., Ruhani, B., 2016. Effects of temperature and nanoparticles concentration on rheological behavior of Fe₃O₄-Ag/ EG hybrid nanofluid: an experimental study. *Exp. Therm. Fluid Sci.* 77, 38–44.
- Akbari, M., Afrand, M., Arshi, A., Karimipour, A., 2017. An experimental study on rheological behavior of ethylene glycol based nanofluid: proposing a new correlation as a function of silica concentration and temperature. *J. Mol. Liq.* 233, 352–357.
- Aly, W.I., 2014. Numerical study on turbulent heat transfer and pressure drop of nanofluid in coiled tube-in-tube heat exchangers. *Energ. Conver. Manage.* 79, 304–316.
- Arani, A.A., Aberoumand, H., Aberoumand, S., Moghaddam, A.J., Dastanian, M., 2016. An empirical investigation on thermal characteristics and pressure drop of Ag-oil nanofluid in concentric annular tube. *Heat Mass Transf.* 52 (8), 1693–1706.
- Asadi, A., Asadi, M., Rezaei, M., Siahmargoi, M., Asadi, F., 2016. The effect of temperature and solid concentration on dynamic viscosity of MWCNT/MgO (20–80)–SAE50 hybrid nano-lubricant and proposing a new correlation: an experimental study. *Int. Commun. Heat Mass Transf.* 78, 48–53.
- Azin, Z., Pourghobadi, Z., 2021. Electrochemical sensor based on nanocomposite of multi-walled carbon nano-tubes (MWCNTs)/ TiO₂/carbon ionic liquid electrode analysis of acetaminophen in pharmaceutical formulations. *Iran. J. Chem. Chem. Eng. (IJCCE)* 40 (4), 1030–1041. <https://doi.org/10.30492/ijcce.2020.39811>.
- Binu, K., Shenoy, B., Rao, D., Pai, R., 2014. A variable viscosity approach for the evaluation of load carrying capacity of oil lubricated journal bearing with TiO₂ nanoparticles as lubricant additives. *Procedia Mater. Sci.* 6, 1051–1067.
- Choi, S.U., Eastman, J.A., 1995. Enhancing thermal conductivity of fluids with nanoparticles. Argonne National Lab, IL (United States).
- Chu, Y.-M., Ibrahim, M., Saeed, T., Berrouk, A.S., Algehyne, E.A., Kalbasi, R., 2021. Examining rheological behavior of MWCNT-TiO₂/5W40 hybrid nanofluid based on experiments and RSM/ ANN modeling. *J. Mol. Liq.* 333, 115969.
- Cui, X., Li, C., Zhang, Y., Said, Z., Debnath, S., Sharma, S., Ali, H. M., Yang, M., Gao, T., Li, R., 2022. Grindability of titanium alloy using cryogenic nanolubricant minimum quantity lubrication. *J. Manuf. Process.* 80, 273–286. <https://doi.org/10.1016/j.jmapro.2022.06.003>.
- Dalkılıç, A., Çebi, A., Celen, A., Yıldız, O., Acıkgoz, O., Jumpholkul, C., Bayrak, M., Surana, K., Wongwises, S., 2016. Prediction of graphite nanofluids' dynamic viscosity by means of artificial neural networks. *Int. Commun. Heat Mass Transf.* 73, 33–42.
- Dardan, E., Afrand, M., Isfahani, A.M., 2016. Effect of suspending hybrid nano-additives on rheological behavior of engine oil and pumping power. *Appl. Therm. Eng.* 109, 524–534.
- Du, X., Tian, W., Pan, J., Hui, B., Sun, J., Zhang, K.,..., Xia, Y. (2022). Piezo-phototronic effect promoted carrier separation in coaxial p-n junctions for self-powered photodetector. *Nano energy*, 92, 106694. doi: 10.1016/j.nanoen.2021.106694.
- Dwijendra, N.K.A., Patra, I., Ahmed, Y.M., et al, 2022. Carbonyl sulfide gas detection by pure, Zn- and Cd-decorated AlP nanosheet. *Monatsh Chem.* <https://doi.org/10.1007/s00706-022-02961-5>.
- Esfe, M. H., Rostamian, H., & Sarlak, M. R. 2018. A novel study on rheological behavior of ZnO-MWCNT/10w40 nanofluid for automotive engines. *Journal of Molecular Liquids*, 254, 406-413.
- Esfe, M. H., Arani, A. A. A., Madadi, M. R., & Alirezaie, A. (2018). A study on rheological characteristics of hybrid nano-lubricants containing MWCNT-TiO₂ nanoparticles. *Journal of Molecular Liquids*, 260, 229-236.
- Esfe, M.H., Alidoust, S., 2020. Experimental evaluation of MWCNT-Al 2 O 3 (40–60%)/5W50 hybrid nanofluid and comparison with MWCNT-Al 2 O 3 (35–65%)/5W50 hybrid nanofluid with focus on thermophysical properties and cost performance index. *Eur. Phys. J. Plus* 135 (10), 1–17.

- Esfe, M.H., Arani, A.A.A., 2018. An experimental determination and accurate prediction of dynamic viscosity of MWCNT (% 40)-SiO₂ (% 60)/5W50 nano-lubricant. *J. Mol. Liq.* 259, 227–237.
- Esfe, M.H., Esfandeh, S., Alidoust, S., Toghrayie, D., 2022. Comparison of viscosity behavior of hybrid nano-lubricants containing Al₂O₃-MWCNT nanoparticles dispersed in SAE XWX engine oils to determine the optimal behavior of nano-lubricants based on experimental studies. *Colloids Surf. A Physicochem. Eng. Asp.* 641, 128446.
- Esfe, M.H., Sarlak, M.R., 2017. Experimental investigation of switchable behavior of CuO-MWCNT (85%–15%)/10W-40 hybrid nano-lubricants for applications in internal combustion engines. *J. Mol. Liq.* 242, 326–335.
- Esfe, M.H., Alidoust, S., Esmaily, R., 2022. A comparative study of rheological behavior in hybrid nano-lubricants (HNLs) with the same composition/nanoparticle ratio characteristics and different base oils to select the most suitable lubricant in industrial applications. *Colloids Surf. A Physicochem. Eng. Asp.* 643, 128658.
- Goharkhah, M., Ashjaee, M., Shahabadi, M., 2016. Experimental investigation on convective heat transfer and hydrodynamic characteristics of magnetite nanofluid under the influence of an alternating magnetic field. *Int. J. Therm. Sci.* 99, 113–124.
- He, W. et al, 2020. Using of artificial neural networks (ANNs) to predict the thermal conductivity of zinc oxide–silver (50%–50%)/water hybrid Newtonian nanofluid. *Int. Commun. Heat Mass Transf.* 116, 104645.
- Jafarimoghaddam, A., Aberoumand, S., 2016. An empirical investigation on Cu/Ethylene Glycol nanofluid through a concentric annular tube and proposing a correlation for predicting Nusselt number. *Alex. Eng. J.* 55 (2), 1047–1052.
- Jayakumar, J., Mahajani, S., Mandal, J., Iyer, K.N., Vijayan, P., 2010. CFD analysis of single-phase flows inside helically coiled tubes. *Comput. Chem. Eng.* 34 (4), 430–446.
- Jia, D., Zhang, Y., Li, C., Yang, M., Gao, T., Said, Z., Sharma, S., 2022. Lubrication-enhanced mechanisms of titanium alloy grinding using lecithin biolubricant. *Tribol. Int.* 169, <https://doi.org/10.1016/j.triboint.2022.107461> 107461.
- Kole, M., Dey, T., 2010. Thermal conductivity and viscosity of Al₂O₃ nanofluid based on car engine coolant. *J. Phys. D Appl. Phys.* 43, (31) 315501.
- Li, H., Zhang, Y., Li, C., Zhou, Z., Nie, X., Chen, Y., Cao, H., Liu, B. o., Zhang, N., Said, Z., Debnath, S., Jamil, M., Ali, H.M., Sharma, S., 2022. Extreme pressure and antiwear additives for lubricant: academic insights and perspectives. *Int. J. Adv. Manuf. Tech.* <https://doi.org/10.1007/s00170-021-08614-x>.
- Liu, K., Zhang, Y., Dai, F., Sun, W., 2021. Improved heat transfer of the engine oil by changing it to hybrid nanofluid: adding hybrid nano-powders. *Powder Technol.* 383, 56–64.
- Mahyari, A.A., Karimipour, A., Afrand, M., 2019. Effects of dispersed added graphene oxide-silicon carbide nanoparticles to present a statistical formulation for the mixture thermal properties. *Physica A* 521, 98–112.
- Mansouri, M., Nademi, M., Ebrahim Olya, M., Lotfi, H., 2017. Study of methyl tert-butyl ether (MTBE) photocatalytic degradation with UV/TiO₂-ZnO-CuO nanoparticles. *J. Chem. Health Risks* 7 (1), 19–32. <https://doi.org/10.22034/jchr.2017.544161>.
- Mirgolbabaei, H., Taherian, H., Domairry, G., Ghorbani, N., 2011. Numerical estimation of mixed convection heat transfer in vertical helically coiled tube heat exchangers. *Int. J. Numer. Meth. Fluids* 66 (7), 805–819.
- Moghadam, M.A., Motahari, K., 2017. Experimental investigation, sensitivity analysis and modeling of rheological behavior of MWCNT-CuO (30–70)/SAE40 hybrid nano-lubricant. *Appl. Therm. Eng.* 123, 1419–1433.
- Nafchi, P.M., Karimipour, A., Afrand, M., 2019. The evaluation on a new non-Newtonian hybrid mixture composed of TiO₂/ZnO/EG to present a statistical approach of power law for its rheological and thermal properties. *Physica A* 516, 1–18.
- PUTRA A.B.W (2020) Computer Technology Simulation towards Power Generation Potential from Coproduced Fluids in South Lokichar Oil Fields. *International Journal of Communication and Computer Technologies*, 8 (2), 9–12. doi:10.31838/ijcccts/08.02.03.
- Rakhsha, M., Akbaridoust, F., Abbassi, A., Majid, S.-A., 2015. Experimental and numerical investigations of turbulent forced convection flow of nanofluid in helical coiled tubes at constant surface temperature. *Powder Technol.* 283, 178–189.
- P. Razi, and M. Akhavan-Behabadi, “Heat Transfer Characteristics of CuO-Base Oil Nanofluid Laminar Flow Inside Flattened Tubes Under Constant Heat Flux.” pp. 591–597.
- Ruhani, B. et al, 2019. Statistical investigation for developing a new model for rheological behavior of Silica–ethylene glycol/Water hybrid Newtonian nanofluid using experimental data. *Physica A* 525, 616–627.
- Ruhani, B. et al, 2019. Statistical investigation for developing a new model for rheological behavior of ZnO–Ag (50%–50%)/Water hybrid Newtonian nanofluid using experimental data. *Physica A* 525, 741–751.
- Ruhani, B. et al, 2022. Statistical modeling and investigation of thermal characteristics of a new nanofluid containing cerium oxide powder. *Heliyon* 8 (11), 11373.
- Shahsavani, E., Afrand, M., Kalbasi, R., 2018. Using experimental data to estimate the heat transfer and pressure drop of non-Newtonian nanofluid flow through a circular tube: applicable for use in heat exchangers. *Appl. Therm. Eng.* 129, 1573–1581.
- Siddiqui, F.R., Tso, C., Chan, K.C., Fu, S.C., Chao, C.Y., 2019. Dataset on critical parameters of dispersion stability of Cu/Al₂O₃ nanofluid and hybrid nanofluid for various ultra-sonication times. *Data Brief* 22, 863–865.
- Sidik, N.A.C., Mohammed, H., Alawi, O.A., Samion, S., 2014. A review on preparation methods and challenges of nanofluids. *Int. Commun. Heat Mass Transf.* 54, 115–125.
- Suhad, H., Neihaya, H., Raghad, A., 2021. Evaluating the biological activities of biosynthesized ZnO nanoparticles using Escherichia coli. *Caspian J. Environ. Sci.* 19 (5), 809–815. <https://doi.org/10.22124/cjes.2021.5221>.
- Sujith, S.V., Solanki, A.K., Mulik, R.S., 2019. Experimental evaluation on rheological behavior of Al₂O₃-pure coconut oil nanofluids. *J. Mol. Liq.* 286, 110905.
- Sujith, S.V., Solanki, A.K., Mulik, R.S., 2021. Experimental investigations on viscosity and density of eco-friendly MoS₂-sesame oil nano-lubricants and its influence on pumping power. *Nanotechnology* 32, (36) 365702.
- Sun, L., Wang, G., Zhang, C., Jin, Q., Song, Y., 2021. On the rheological properties of multi-walled carbon nano-polyvinylpyrrolidone/silicon-based shear thickening fluid. *Nanotechnol. Rev. (Berlin)* 10 (1), 1339–1348. <https://doi.org/10.1515/ntrev-2021-0087>.
- Tang, Z., Qi, C., Tian, Z., Chen, L., 2022. Thermal management of electronic components based on new wave bio-inspired structures and nanofluids. *Int. Commun. Heat Mass Transf.* 131, 105840.
- Tassew, M.F., Chouhan, G., Tsegaye, M.M., Tyagi, P., 2022. Green synthesized metallic nanoparticles as prospective therapeutics in fight against listeria monocytogenes. *Eur. Chem. Bull.* 11 (3), 14–33. <https://doi.org/10.31838/ecb/2022.11.03.003>.
- Tian, X.-X., Kalbasi, R., Qi, C., Karimipour, A., Huang, H.-L., 2020. Efficacy of hybrid nano-powder presence on the thermal conductivity of the engine oil: an experimental study. *Powder Technol.* 369, 261–269.

- Tu, J., Fan, F., Qi, C., Ding, Z., Liang, L., 2022. Experimental study on the particle fouling properties of magnetic nanofluids in a corrugated tube with built-in twisted turbulator under variable magnetic field. *Powder Technol.* 400, 117216.
- Tu, J., Qi, C., Li, K., Tang, Z., 2022. Numerical analysis of flow and heat characteristic around micro-ribbed tube in heat exchanger system. *Powder Technol.* 395, 562–583.
- Tu, J., Qi, C., Tang, Z., Tian, Z., Chen, L., 2022. Experimental study on the influence of bionic channel structure and nanofluids on power generation characteristics of waste heat utilisation equipment. *Appl. Therm. Eng.* 202, 117893.
- Wang, M., Deng, L., Liu, G., Wen, L., Wang, J., Huang, K.,..., Pan, Y. (2019). Porous Organic Polymer-Derived Nanopalladium Catalysts for Chemoselective Synthesis of Antitumor Benzofuro[2,3 b]pyrazine from 2 Bromophenol and Isonitriles. *Organic letters*, 21(13), 4929-4932. doi: 10.1021/acs.orglett.9b01230.
- Wang, X., Li, C., Zhang, Y., Ali, H.M., Sharma, S., Li, R., Yang, M., Said, Z., Liu, X., 2022. Tribology of enhanced turning using biolubricants: a comparative assessment. *Tribol. Int.* <https://doi.org/10.1016/j.triboint.2022.107766> 107766.
- Wang, Y., Qi, C., Zhao, R., Wang, C., 2022. Study on the mechanism of modified surface and magnetic nanofluids on cooling performance of wireless charging equipment under magnetic field. *Appl. Therm. Eng.* 208, 118258.
- Wenhao Xu, Changhe Li, Yanbin Zhang, Hafiz Muhammad Ali, Shubham Sharma, Runze Li, Min Yang, Teng Gao, Mingzheng Liu, Xiaoming Wang, Zafar Said, Xin Liu, Zongming Zou. 2022. Electrostatic atomization minimum quantity lubrication machining: from mechanism to application. *Int. J. Extrem. Manuf.* <https://doi.org/10.1088/2631-7990/ac9652>.
- Yang, L., Huang, J.-N., Mao, M., Ji, W., 2020. Numerical assessment of Ag-water nanofluid flow in two new microchannel heatsinks: thermal performance and thermodynamic considerations. *Int. Commun. Heat Mass Transf.* 110, 104415.
- Yang, M., Li, C., Zhang, Y., Jia, D., Zhang, X., Hou, Y., Li, R., Wang, J., 2017. Maximum undeformed equivalent chip thickness for ductile-brittle transition of zirconia ceramics under different lubrication conditions. *Int. J. Mach. Tool Manu.* 122, 55–65. <https://doi.org/10.1016/j.ijmachtools.2017.06.003>.